



ELSEVIER

Earth and Planetary Science Letters 167 (1999) 335–345

EPSL

Trace element distributions in the chalcopyrite wall of a black smoker chimney: insights from laser ablation inductively coupled plasma mass spectrometry (LA–ICP–MS)

I.B. Butler*, R.W. Nesbitt

Department of Geology, Southampton Oceanography Centre, University of Southampton, Empress Dock, European Way, Southampton, SO14 3ZH, UK

Received 10 February 1999; accepted 22 February 1999

Abstract

The thin walls of young black smoker chimneys experience steep physico-chemical gradients during active venting of hydrothermal fluid, and these gradients control trace element precipitation within those walls. Here, we utilise a combination of high sensitivity ICPMS and UV laser ablation (resolution of better than 30 μm) to demonstrate the existence of non-random V, Ag, In, Te, Ba, Au, Pb and U distributions within the chalcopyrite wall of an immature black smoker chimney. The data are the first of their kind to be produced for black smoker chimney walls. Distributions of In and Te are attributed to preferential incorporation into lattices at elevated temperature. Enrichments of U and V derived from seawater are the product of redox immobilisation on sulphide surfaces. The distributions of Au, Ag, Pb and Ba may be related to interactions at the hydrothermal fluid–seawater mixing front; however, comparison of distribution data with reaction-transport models of chimney walls suggest a possible pH control on precipitation. These data illustrate the power of the LA–ICP–MS method, and such spatially resolved data have the potential to constrain models of element precipitation both in chimneys and in associated mounds. © 1999 Elsevier Science B.V. All rights reserved.

Keywords: trace elements; sulfides; hydrothermal vents; laser methods; inductively coupled plasma methods; mass spectroscopy

1. Introduction

The thin walls of active black smoker chimneys are permeable and separate fluids extremely different from each other in terms of temperature, composition and redox state. Thus, young black smoker chimney

walls experience steep physico-chemical gradients at scales of less than 10 mm. Studies of sulphur isotope distributions (e.g. [1]) have revealed systematic variations of $\delta^{34}\text{S}$ in black smoker structures at scales of 60 μm to 1 mm. This study demonstrates similarly systematic trace element variations at sub-mm scales.

Chimney growth is initiated by focused venting of $\sim 350^\circ\text{C}$ hydrothermal fluid from a fracture on the seafloor or in a sulphide mound [2]. Mixing of hydrothermal fluid and seawater at temperatures

* Corresponding author. Present address: Department of Earth Sciences, Cardiff University, Park Place, Cardiff CF1 3YE, Wales, UK. Tel.: +44-1222-874830; Fax: +44-1222-874326; E-mail: butlerib@cardiff.ac.uk

of $>150^{\circ}\text{C}$ causes supersaturation and precipitation of anhydrite [3] which provides structural support and sites for sulphide nucleation. Precipitation of chalcopyrite produces a sulphide conduit lining, and advection of hydrothermal fluid through the permeable wall causes replacement of anhydrite by chalcopyrite, and overgrowth of earlier-formed sulphides. Detailed modelling of reaction-transport processes within chimney walls [4,5] has enhanced our understanding of the development of mineralogical zoning of those walls. Trace element precipitation is sensitive to a variety of geochemical factors, and distributions will elucidate details of fluid interactions within chimney walls. This assertion is supported by studies [6,7] of major and minor element zoning in thick-walled, mature chimneys which relate elemental distributions to seawater and hydrothermal fluid mixing. In juvenile, thin-walled, structures, the fine-scale relationship of trace elements to sites of fluid interaction remains unknown, largely because of the lack of routine analytical methods which combine sub-100 μm spatial resolution with sub- $\mu\text{g g}^{-1}$ detection limits.

Conventional bulk analysis methods homogenise fine-scale geochemical signatures. Here, we utilise a combination of Nd-YAG UV laser ablation with a high-sensitivity ICP-MS allowing rapid sampling at resolutions of better than 30 μm and with detection limits of 10–100 ng g^{-1} for elements such as V, Ag, In, Te, Ba, Au, Pb, and U in sulphide. The data are the first of their kind to be reported from sea-floor sulphide materials. A preliminary qualitative interpretation of the trace element distributions is presented herein, although further developments in LA-ICP-MS methodology are required before fully quantitative data can be produced to provide important constraints for geochemical models.

2. The black smoker chimney

The tip of the small chimney studied here (Fig. 1) is part of a major active chimney structure from the Broken Spur vent field ($29^{\circ}10'\text{N}$, MAR). Observations from submersibles indicate that the major structure had grown by about 4 m in 18 months and the size and position of the sample suggests that it represents a very short growth period (days or weeks).

The reader is referred to the literature for further details of the vent field itself [8–11]. The chimney tip is a thin-walled (~ 8 mm) ‘organ pipe’ structure composed of three major mineralogical zones (Fig. 1). Zone A is a 2–3 mm thick inner monomineralic chalcopyrite conduit lining. Zone B is situated outside of zone A and is a 1–2 mm thick zone of chalcopyrite overgrowing minor ($<10\%$) euhedral pyrite and anhedral sphalerite. The transition between zones A and B is sharp and occurs over <100 μm . The outer edge of zone B is a thin discontinuous zone of localised modification of chalcopyrite to bornite \pm chalcocite/digenite. The anhydrite wall of the chimney is represented by zone C. Euhedral pyrite within zone C is texturally identical to pyrite in zone B. Outward fingering of chalcopyrite and secondary Cu sulphides is consistent with anhydrite replacement by Cu sulphides along grain edges. Visual estimates suggest that there is about 10% porosity within the chimney, much of which is connected and likely facilitates fluid–materials transport across the wall. The mineralogical succession is simple: anhydrite + pyrite + sphalerite \rightarrow chalcopyrite \pm isocubanite \rightarrow bornite \rightarrow chalcocite/digenite \rightarrow covellite \rightarrow Fe oxyhydroxides.

3. Methods

The instrumentation is a combination of a VG Elemental Plasmaquad PQ2+ ICP-MS coupled to a frequency quadrupled Spectron Systems Nd-YAG UV laser operating at 266 nm [12]. The tiny quantities of analyte recovered from $\sim 20 \times 45$ μm deep ablation pits represent only 7×10^{-5} g of material and require high sensitivity for analysis at sub- $\mu\text{g g}^{-1}$ levels. Modifications of the basic instrumentation and operating conditions [12,13] result in a machine with sensitivities of 1×10^9 cps μg^{-1} g^{-1} in solution mode or 2000–20,000 cps μg^{-1} g^{-1} in laser mode, subject to matrix. A laser power of 2 mJ at 266 nm gave ~ 20 μm diameter ablation pits with a drilling rate of 2–3 $\mu\text{m s}^{-1}$ and provided an optimal balance between instrumental sensitivity and signal stability. Drifts in instrumental sensitivity during an analytical run were monitored by analysis of NIST612. Operating conditions for the ICP-MS and the laser are shown in Table 1.

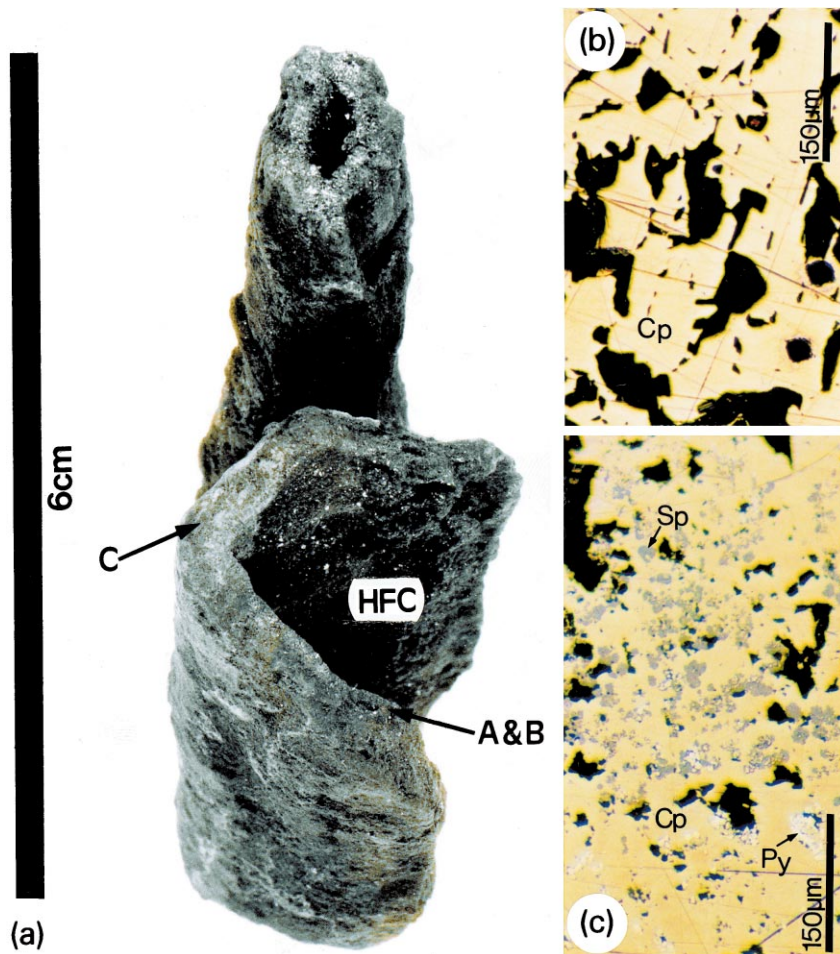


Fig. 1. The black smoker chimney. (a) The black smoker chimney tip, the relative positions of mineralogical zones A, B and C, and the hydrothermal fluid conduit (HFC). Polished sections for LA-ICP-MS analysis were taken from the base of this sample. (b) Typical textures from monomineralic zone A. Chalcopyrite (Cp) is the only mineral present and the zone shows significant porosity. (c) Zone B sulphide. Chalcopyrite is the major mineral within this zone; however, in this image, pyrite (Py) and sphalerite (Sp) are present as significant components of the assemblage.

For analysis, linear profiles of ablation pits were made running from the inner conduit lining to the outer limit of zone B (Fig. 1). Anhydrite has uneven ablation characteristics, and was not routinely analysed. Analytical blanks were obtained by measurement of the Ar/N₂ carrier gas. Analysis utilised peak jump mode with a 5 s pre-ablation period followed by a 15 s acquisition time. For each analytical run, a total of ~16 isotopes were analysed. The choice of elements for analysis was driven both scientifically and methodologically. For example, some of the elements (e.g. In, Te, Ag) were chosen because

it is known that they partition into sulphide lattices, whilst others (e.g. major elements) are present at too high a concentration for LA-ICP-MS analysis. Other elements of interest (e.g. Se) are subject to major isobaric interference, and so were not analysed.

Certified matrix-matched standards for sulphides which are homogeneous at 20 μm scales do not currently exist [13]. Consequently, deriving quantitative compositional data is problematic. Nevertheless, for this type of study the trace element distribution patterns hold as much interest as do the absolute concentration values. LA-ICP-MS has the virtue of

Table 1
Standard operating conditions for the LA–ICP–MS used during the analysis of sulphides

Operating conditions used for spectron systems Nd-YAG UV laser and VG Elemental Plasmaquad PQ2+ ICP–MS:	
Laser source	
Laser beam	UV 266 nm frequency quadrupled Nd-YAG
Mode	Q-switched pulse
Pulse duration	5–10 ns
Repetition rate	6.5 Hz
Power	100 mJ (1064 nm), 2 mJ (266 nm)
Preablation time	5 s
Acquisition time	15 s
Pit diameter	~20 μm (in sulphide)
Inductively coupled plasma mass spectrometer	
<i>Plasma conditions</i>	
RF power	1.35 kW forward, <2 W reflection
Cool gas flow	Ar 14.0 l min ⁻¹
Auxiliary gas flow	Ar 1.1 l min ⁻¹ (aux. 1.0 l min ⁻¹)
Nebuliser gas flow	Ar 1.0 l min ⁻¹
N ₂ mixing gas	0.4 ml min ⁻¹
<i>Vacuum interface</i>	
Expansion chamber	7.0 \times 10 ⁻¹ mbar (with S-option rotary pump)
Intermediate stage	<10 ⁻⁴ mbar
Analyser	3.5 \times 10 ⁻⁶ mbar
Sampling cone	Ni 1.0 mm aperture
Skimmer cone	Ni 0.7 mm aperture
<i>Acquisition parameters</i>	
Detector type	Galileo Channeltron
Ion detection	Pulse counting
Scanning mode	Peak jump, 3 points/peak (ΔM 0.069 amu)
Dwell time	10.24 ms
DAC/step	5
Quad settle time	10 ms

linear sensitivity over most of its dynamic range, and so trace element trends and enrichment factors can be determined on the basis of the detector response alone. However, instrumental sensitivity is not flat across the mass range studied (51–238 amu) and this is accentuated by the Fisons ‘S’ interface

which produces a steep-sided mass response curve with peak sensitivity at the tuning mass [13]. Only isotopes of very similar mass are comparable in concentration terms on the basis of uncalibrated detector response. In order to broadly quantify trace element concentrations in the chimney wall, bulk analysis was also carried out using conventional solution ICP–MS methods, after complete sample digestion in aqua regia. For this, the outer anhydrite zone was carefully removed using an engraving tool in order that the bulk analysis of the chalcopyrite wall matched the LA–ICP–MS analysis.

4. Results and discussion

Distributions of V, Ag, In, Te, Ba, Au, Pb, and U from two traverses across the chimney wall are shown in Fig. 2. Maximum and minimum detector responses for the profiles and bulk geochemical data (obtained after bulk digestion) for the chimney are shown in Table 2. In the absence of matrix-matched ablation standards it is not possible to provide a quantitative analysis for each element on the profile. However, we stress the point that the value of the patterns lies in their relative distribution, and since LA–ICP–MS has linear sensitivity, it is possible to estimate enrichment factors from the raw data alone. Note that all the analyses were made within a chalcopyrite matrix and so the variation observed in the profiles is not a major function of bulk mineralogy.

The bulk trace element data for most elements discussed here fall well within the range of analyses reported from chimneys recovered from a number of hydrothermal fields [14]. The exception to this rule would appear to be Te (45 $\mu\text{g g}^{-1}$), the concentration of which appears to be higher than is usually observed for sea-floor sulphide materials (typically <10 $\mu\text{g g}^{-1}$). However, Te concentrations of the order reported here are not unprecedented, and bulk geochemical data for massive sulphides from EPR

Fig. 2. Distribution data obtained on two profiles through the wall of a young black smoker chimney. Each analysis is presented as a percentage of the maximum detector response recorded on each profile (the relative response). This is a common method used to show uncalibrated LA–ICP–MS data [26]. The ‘position on profile’ is the number of the ablation analyses taken across the chimney wall. (A) In and Te (profile 12). (B) In and Te (profile 8). (C) U and V (profile 12). (D) U (profile 8). (E) Ag and Au (profile 12). (F) Ag and Au (profile 8). (G) Pb (profile 8). (H) Ba (profile 8). The figure below each column shows the mineralogical zones of the chimney wall. HFC = hydrothermal fluid conduit.

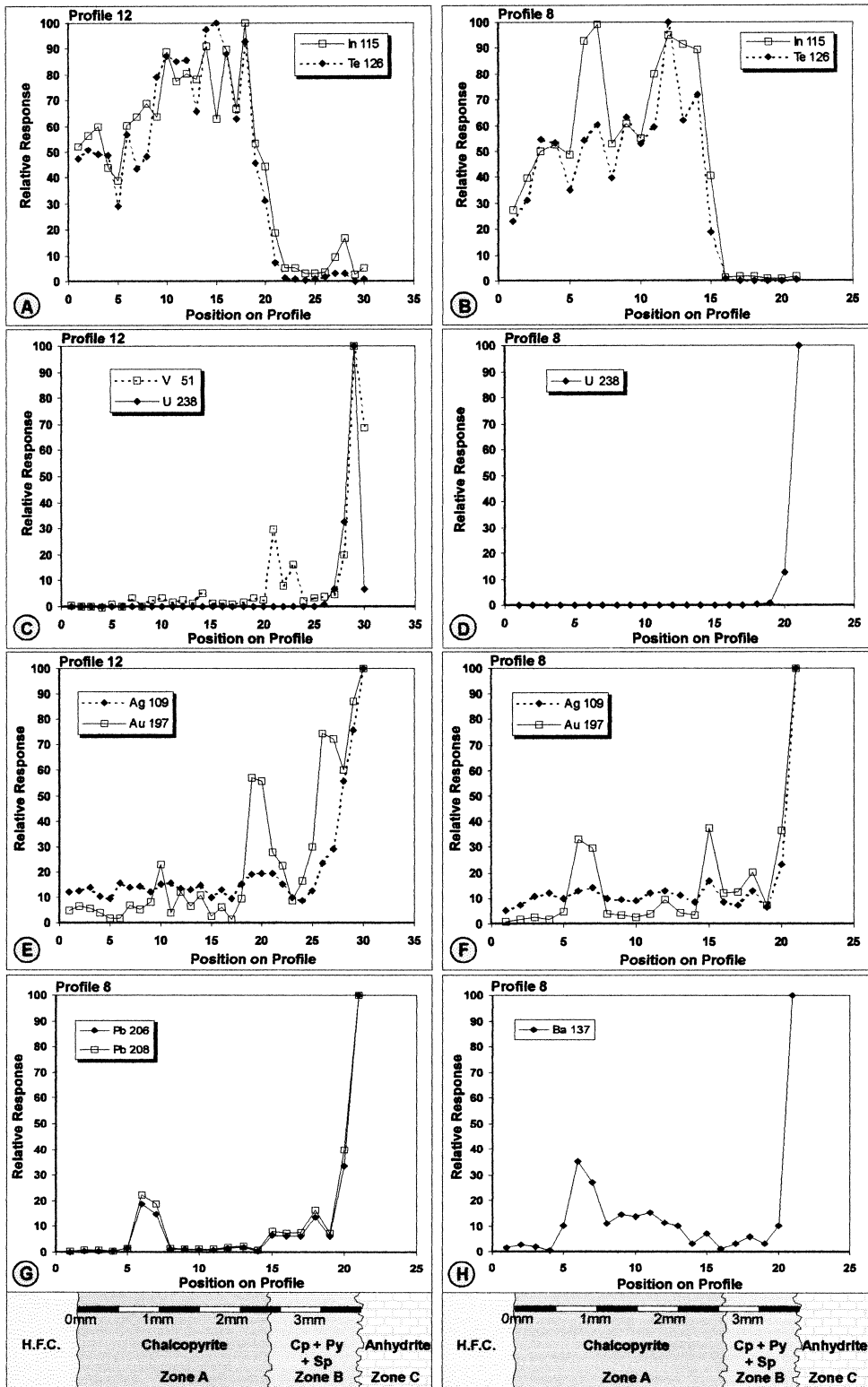


Table 2

Maximum and minimum counts per second (cps) for each isotope analysed on profiles 8 and 12

Isotope	Bulk wall (ppm)	Analytical profile 8		Analytical profile 12	
		maximum cps	minimum cps	maximum cps	minimum cps
⁵¹ V	13			127,844	0
¹⁰⁷ Ag	27	188,898	9,274	441,147	39,256
¹⁰⁹ Ag	27	205,489	10,377	435,530	38,138
¹¹⁵ In	2	30,034	211	61,474	1,546
¹²⁵ Te	45	36,630	28	98,084	65
¹²⁶ Te	45	100,253	5	264,613	454
¹³⁷ Ba	8	7,114	40		
¹⁹⁷ Au	0.5	4,368	28	9,691	129
²⁰⁶ Pb	9	1,352,786	2,028		
²⁰⁸ Pb	9	2,317,641	4,920		
²³⁸ U	2	461,190	25	829,992	9

Bulk compositions determined by solution ICP–MS.

13°N and Galapagos Rift [14] are in the range 10–20 $\mu\text{g g}^{-1}$, whilst μPIXE analysis by the same worker returns spot values for Te in massive pyrite of up to 260 $\mu\text{g g}^{-1}$.

4.1. Chimney growth and trace element distributions

The structure of the chimney is shown in Fig. 1 and a comparison between Tivey's modelled chimney wall chemistry and our data is shown in Fig. 3. Zone A is monomineralic chalcopyrite, and textures suggest that zone B has developed by replacement of the anhydrite wall. Therefore, the zone A–B transition is interpreted as the position of the original conduit wall (Fig. 3). Sulphide growth initiated at this surface occurs in two directions: inwards, forming zone A, and outwards, developing zone B. Reaction-transport modelling [5] suggests that bulk mineralogical zoning of chimney walls is determined principally by temperature and to a lesser extent by pH and that mineral stability in vent fluids under in-situ conditions is insensitive to redox equilibria within H_2 concentration ranges of several orders of magnitude. However, it also appears to be true that bornite–chalcopyrite and, possibly, pyrite–pyrrhotite relations in many black smokers can reflect changing redox conditions. What is evident from previous studies [7,15] is that, unlike bulk mineralogy, redox processes can be a major control for trace element distributions. The novelty of the data presented here is that they are the first demonstration of the shape and

form of the distribution patterns which are produced by temperature, redox and fluid mixing controls. This knowledge of the shape and form of the patterns al-

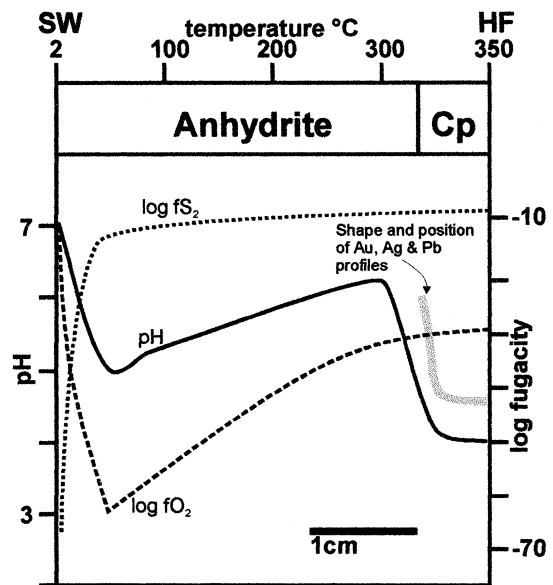


Fig. 3. Modelled redox and pH profiles across a two-layer chimney wall using hydrothermal fluid (HF) from Vent 4 (11°N, EPR) and seawater (SW) as fluid end-members. The modelled data are from Tivey [5]. Superimposed is the position and form of typical Au, Ag and Pb concentration profiles measured within the Broken Spur chimney. The shape of the trace element and pH profiles within the chalcopyrite wall are similar and it is possible that Au, Ag and Pb precipitation may be controlled by pH gradients.

lows us to compare our results with pH and redox gradients predicted by reaction-transport modelling.

Three trace element distribution styles were found (Fig. 2). Type I distribution displayed by Te and In is characterised by enrichment within zone A and total absence in zone B. Type II distribution, shown by U and V, is typified by major enrichments (up to 10^5 times) in the very outer part of the sulphide wall. Type III distribution, shown by Au, Ag, Pb and Ba, is characterised by major enrichments within zone B, particularly close to the anhydrite–sulphide contact, but unlike type II (U and V), these elements are found sporadically in zone A.

4.2. Tellurium and indium

Te and In display progressively elevated concentrations from the central wall of the chimney, outward up to the zone A–B transition. At this boundary, concentrations fall to background levels over a distance of $<100 \mu\text{m}$. The coincidence of a sharp mineralogical transition with maximum and minimum values for Te and In must reflect the processes controlling the precipitation of these elements. Based on size and valency arguments, Te and In can substitute for S^{2-} and Fe^{3+} (respectively) in the chalcopyrite structure. Te^{2-} is 16% larger [16] than S^{2-} , and In^{3+} is about 20% larger than Fe^{3+} [17], suggesting that substitution will be favoured by high temperatures. Further evidence that substitution is possible is the fact that Te^{2-} has been recorded as substituting for S^{2-} in pyrite [18] and rosquesite (CuInS_2) which is isostructural with chalcopyrite [19].

As previously stated, we interpret the zone A–B transition as the point of initiation of the sulphide wall, with zone A representing high-temperature inward growth of chalcopyrite and zone B representing lower-temperature outward replacement of the anhydrite wall. If this model is correct then the distribution of In and Te may be a function of temperature with the rapid climb in concentration of these elements representing a zone where conditions are ideal for substitution. The sharp transition ($<100 \mu\text{m}$) from maximum to minimum abundance of these elements in the outer parts of the chalcopyrite wall is explained when the growth history of the chimney wall is considered. We propose a model in which the differing mechanisms of sulphide formation in

zones A and B account for the distribution of Te and In in the two zones. In zone A, Te and In are co-precipitated with S and Fe during high-temperature primary growth of chalcopyrite, whilst in zone B chalcopyrite has a replacive, probably lower-temperature, origin and as such the significantly larger size of Te and In precludes them from the structure. Such dependence of trace element partitioning between a mineral lattice and a fluid on temperature is a common phenomenon in mineral chemistry.

4.3. Uranium and vanadium

The contrasting behaviour of U and V in seawater and hydrothermal solutions is well documented [20]. Seawater U concentrations are close to 14 nmol l^{-1} [20]; however, circulation of seawater through basaltic crust results in quantitative extraction of the element and fluid expelled at oceanic ridge-crest systems is essentially free of U [20]. Hence, U and V (which mimics U) observed in the outer parts of zone B are derived from seawater. The reduced solubility of both U and V under reducing conditions points to a redox control on their precipitation in the chimney wall.

Since the U and V enrichments occur close to the chalcopyrite–anhydrite boundary in the chimney wall, it was considered that a possible source of enrichment could come from sub-sampling of seawater-derived anhydrite during analysis. The laser pit is large enough to be able to intersect small grains of anhydrite mixed in with chalcopyrite close to the zone boundary. Analysis of pure anhydrite produced detector responses two or more orders of magnitude less than those recorded for the U and V maxima in the chalcopyrite wall. Thus the high levels of U and V found in the outer parts of zone B are not the result of anhydrite contamination of the analysis, and are products of seawater incursion into the outer part of the chimney wall. We envisage a process analogous to that which occurs at the oxic–post-oxic boundary in deep-sea sediments [21] where U and V are concentrated by an efficient redox trap mechanism. However, it is unlikely that U and V substitute into the sulphide lattice (as appears to be the case for In and Te), and it is probable that concentrations of both U and V occur over grain surfaces, although whether this process is mediated by bacteria or inor-

ganic means is unclear from our study. Enrichment of U by microbial process at pyrite grain surfaces has been documented [20] by studies of metalliferous sediments from the TAG hydrothermal field. In this situation, however, the U enrichments are associated with oxide coatings on the pyrite grain surfaces, but for the chimney studied herein, no such oxide coatings are observed in association with any part of the chalcopyrite wall. Experimental studies of the interaction between U(VI) in solution and sulphide mineral surfaces [22] provide evidence for sorption and reduction of U(VI) to U(V) on those surfaces. The interaction of U(VI) with pyrite and galena surfaces has been examined [22], although no data are available for chalcopyrite. However, there is no reason to suppose that chalcopyrite would not also be able to immobilise U(VI) over grain surfaces. Once fixed on the sulphide, the very low solubility of U and V under the prevailing reducing conditions ensures that they remain fixed.

4.4. Gold, silver, lead and barium

Unlike U and V, the source of Au, Ag, Pb and Ba is from hydrothermal fluid. In the studied chimney, the highest concentration of these elements occurs in the same zone as U and V. Additionally, Au, Ag, Pb and Ba occur sporadically in zone A, where U and V fall below the detection limits of the instrument. Although this group of elements show similar distributions within the chalcopyrite wall of the chimney, the siting of the elements within the wall is likely to be very different. Clearly, Ba will not substitute in the chalcopyrite lattice, and is present as sub-microscopic inclusions of barite. Thus the observed trace element pattern can be attributed to barite precipitation where hydrothermal fluid and seawater mix. The erratic distribution of Au within zone B also suggests that Au is present as sub-microscopic inclusions and not as a lattice substitution into chalcopyrite. Ion probe analysis of chalcopyrite from ancient VHMS deposits [18] suggests that Pb is present as inclusions rather than as lattice substitutions. Similarly, it is likely that in the chimney wall Pb is present as submicroscopic grains within the chalcopyrite. By contrast to the three elements discussed above, Ag commonly occurs as a lattice substitution for Cu in chalcopyrite [18,23]. However, the distribution of

the element in the chimney wall is similar to Pb, and it is possible that Ag could also be present as submicroscopic grains of argentiferous galena.

In hydrothermal solution, Au can be transported as a chloro-complex [24] but it is more likely that in sulphide bearing solutions at temperatures of less than 350–400°C, it is transported as bisulphide complexes [7,15,25,26,29], either $\text{Au}(\text{HS})_2^-$ or AuHS^0 [26]. By contrast, Ag is usually transported as chloro-complexes, and for the SW vent at 21°N EPR ($\text{Cl}^- = 494 \text{ mmol kg}^{-1}$, $\text{H}_2\text{S} = 7.1 \text{ mmol kg}^{-1}$ [27]) the Ag speciation is calculated as AgCl_2^- -dominated [6]. Measured fluid data and venting temperatures from Broken Spur [28] are similar to those from the SW vent ($\text{Cl}^- = 505 \text{ mmol kg}^{-1}$, $\text{H}_2\text{S} = 9.3 \pm 1.7 \text{ mmol kg}^{-1}$, temperature $\approx 360^\circ\text{C}$), and AgCl_2^- is expected to be dominant. Similar arguments apply to Pb, which also must be transported as a chloro-complex.

In view of the manner by which Au, Ag and Pb are transported in hydrothermal solution, we suggest two possible processes for enrichment within zone B and at the zone B–C contact. Firstly, we predict that precipitation can be caused both by cooling and oxidation [7,15,25], particularly for Au, where oxidation of the bisulphide complex means that Au is unable to remain in solution. The most probable mechanism for this is by fluid mixing and this is consistent with the zone of highest concentration being the outer edge of the sulphide wall of the chimney. However, Au, Ag and Pb are also found within zone A, which is perhaps an indication that seawater penetration into the chimney is further than that indicated by U and V. Thus, the sporadic nature of the Au, Ag and Pb distribution in zone A may reflect the irregular permeability of the chimney wall with access of seawater into zones close to the conduit depending upon fluctuating pressure of the hydrothermal fluid over the chimney wall.

A second possible explanation arises from comparison of our data with the results of reaction-transport modelling of fluid interactions across chimney walls. As well as predicting the bulk mineralogy of chimney walls, the reaction-transport modelling of Tivey [5] also predicts the form of redox ($f\text{S}_2$ and $f\text{O}_2$) and pH gradients across the wall. For the cases of In, Te, V, and U the distribution patterns observed in the chimney wall show no immediate or simple re-

relationship to modelled redox or pH gradients within the wall, and their distributions can be attributed to temperature controls on lattice substitution and to localised sorption and reduction on sulphide grain surfaces. However, for elements such as Au, Ag, and Pb, there is a clear similarity between observed distribution patterns and predicted pH gradients within the chalcopyrite zone of the chimney wall (Fig. 3). Tivey [5] has shown that redox and pH gradients across chimney walls are best modelled as a function of three major controls: fluid composition, the structure of the wall, and the rate of advection of hydrothermal fluid and seawater across the wall. Of the several examples modelled by Tivey, the cases with the closest fluid composition to Broken Spur [28] are the two- and three-layer models from the SW vent (EPR 21°N) and Vent 4 (EPR 11°N). In these examples, Tivey [5] modelled with and without fluid or seawater advection (figs. 5 and 7 in reference 5; Fig. 3 herein) and showed that the greatest difference occurred where there was outward advection of hydrothermal fluid. In non-advection or seawater advection cases, the greatest changes occur close to the seawater contact where fS_2 drops and fO_2 rises dramatically. The fO_2 pattern is mirrored by the pH. In these cases there appears to be no spatial correlation between these trends and the distributions for Au, Ag and Pb as shown by the Broken Spur chimney. However, where there is hydrothermal fluid advection across the chimney wall, Tivey has modelled an abrupt pH change of 3–4 log units from acid to neutral or slightly alkaline close to the chalcopyrite–anhydrite transition. This is exactly where we observe the major concentration changes for Ag, Au and Pb within the Broken Spur chimney. It is important to note that in the hydrothermal fluid advection model there is no corresponding variation in either fS_2 or fO_2 at the point where the pH transition occurs. Hence, rather than oxidation being the prime control over Au precipitation in chimney walls [7,15,25], it would appear that the major control may be pH.

This conclusion, drawn from the comparison of modelled pH gradients and measured trace element distributions, requires that hydrothermal fluid be advected outward through the chimney wall, and this is consistent with the structure of the wall. Textural evidence from the wall suggests outward growth of

the chalcopyrite inner wall by replacement of anhydrite, and the enrichment of trace elements which must be sourced from hydrothermal fluid in the outer part of zone B clearly indicates outward advection of hydrothermal fluid. However, U and V can only be derived from seawater, and major enrichments of U and V within the outer part of the sulphide wall can only indicate inward advection of seawater into the outer part of the wall. Mineralogical observations suggest that predicted reaction-transport models of fluid interactions in chimney walls [5] are close approximations to natural situations. For some modelled cases our trace element data can be reconciled with predicted pH gradients across the wall. However, it is clear from the trace element data presented here and from mineralogical relationships (e.g. chalcopyrite–bornite textures) that inward advection of seawater produces geochemical and mineralogical features in walls which also show clear evidence for outward advection of hydrothermal fluid. When we consider the evolution of a black smoker chimney, the above evidence suggests an early phase of growth with a porous chalcopyrite wall and outward advection of hydrothermal fluid as a dominant process. Precipitation of sulphides and reduction of porosity would be expected to reduce outward fluid advection, and so with time, inward advection of seawater would become dominant within the outer parts of the chimney wall. Hence, trace element distribution patterns for In, Te, Pb, Ag and Au would be developed as outward advection of hydrothermal fluid is dominant, and U, V and Ba distributions would be expected to develop as inward advection of seawater became possible at a later phase in the development of the chimney. Hence, our trace element data suggest that a future direction for reaction-transport modelling would be to consider the result of a progressive change of fluid transport directions across the wall over time caused by progressive mineral precipitation–dissolution and consequent changes in porosity.

5. Conclusions

This contribution presents the first data on metal distribution at the micro-scale across a young black smoker chimney which allows interpretation of con-

trols of metal distribution. Within the sulphide wall of the chimney In, Te and Ag are present as substitutions into the chalcopyrite lattice, U and possibly V are immobilised on sulphide surfaces and Au, Pb and Ba are present as submicroscopic mineral grains. All of the above elements show systematic distribution patterns, and despite differences in the siting of elements, a limited variety of distribution patterns are observed in the chimney wall. Knowledge of fluid chemistry allows us to determine that the observed patterns are the result of interactions of both seawater and hydrothermal fluids with each other and with mineral surfaces within the chimney wall. Comparison of measured data with reaction-transport models indicates that under certain fluid advection conditions, and with particular fluid compositions, some trace element patterns (e.g. Au, Ag, Pb) are mimicked by pH gradients within the inner part of the wall, and we suggest that pH gradients may control trace element precipitation in some chimneys.

The measured trace element patterns allow us to discern fluid advection directions within the wall, and provide evidence for both outward hydrothermal fluid advection and inward seawater advection, as do mineralogical and textural observations. This feature is consistent with evolution of fluid migration regimes in chimney walls over time, almost certainly in response to porosity and permeability changes caused by mineral precipitation. A possible future direction for reaction-transport modelling is to consider changes in permeability as a result of mineral precipitation, and thus changes in rates and direction of fluid migration in chimney walls.

Acknowledgements

The work presented here was supported by NERC research grants GR9/02760 and GST/02/976. The black smoker chimney in question was recovered by the BRAVEX/94 research cruise aboard R/V *Akademik Mstislav Keldysh* and the authors acknowledge the master Yuri Gorbach and the crew of that vessel. Thanks to Andy Milton for his expertise in LA-ICP-MS analysis. Finally, both authors would like to thank Mark Hannington and other anonymous reviewers for their help in improving the original draft of this paper. [MK]

References

- [1] D.E. Crowe, J.W. Valley, Laser microprobe study of sulphur isotope variation in a seafloor hydrothermal spire, Axial Seamount, Juan de Fuca Ridge, eastern Pacific, *Chem. Geol.* 101 (1992) 63–70.
- [2] R.M. Haymon, Growth history of hydrothermal black smoker chimneys, *Nature* 301 (1983) 695–698.
- [3] C.W. Blount, F.W. Dickson, The solubility of anhydrite (CaSO₄) in NaCl–H₂O from 100 to 450°C and 1–1000 bars, *Geochim. Cosmochim. Acta* 33 (1969) 227–245.
- [4] M.K. Tivey, R.E. McDuff, Mineral precipitation within the walls of black smoker chimneys: a quantitative model of transport and chemical reaction, *J. Geophys. Res.* 95 (1991) 12617–12637.
- [5] M.K. Tivey, The influence of hydrothermal fluid composition and advection rates on black smoker chimney mineralogy: insights from modelling transport and reaction, *Geochim. Cosmochim. Acta* 59 (1995) 1933–1950.
- [6] R. Moss, S.D. Scott, Silver in sulphide chimneys and mounds from 13°N and 21°N, East Pacific Rise, *Can. Mineral.* 34 (1996) 697–716.
- [7] P.M. Herzig, M.D. Hannington, Y. Fouquet, S.U. Von Stakelburg, S. Petersen, Gold-rich polymetallic sulphides from the Lau back arc and implications for the geochemistry of gold in seafloor hydrothermal systems of the southwest Pacific, *Econ. Geol.* 88 (1993) 2182–2209.
- [8] B.J. Murton, C. Van Dover, E. Southward, Geological setting and ecology of the Broken Spur hydrothermal vent field: 29°10'N on the Mid-Atlantic Ridge, in: L.M. Parson, C.L. Walker, D.R. Dixon (Eds.), *Hydrothermal Vents and Processes*, Geol. Soc. London, Spec. Publ. 87 (1995) 33–42.
- [9] R.W. Nesbitt, The geology of the Broken Spur hydrothermal vent field: a new look at an old field, *BRIDGE Newsl.* 8 (1995) 30–34.
- [10] R.C. Duckworth, R. Knott, A.E. Fallick, D. Rickard, B.J. Murton, C. Van Dover, Mineralogy and sulphur isotope geochemistry of the Broken Spur sulphides, 29°N, Mid-Atlantic Ridge, in: L.M. Parson, C.L. Walker, D.R. Dixon (Eds.), *Hydrothermal Vents and Processes*, Geol. Soc. London, Spec. Publ. 87 (1995) 175–189.
- [11] I.B. Butler, A.E. Fallick, R.W. Nesbitt, Mineralogy, sulphur isotope geochemistry and the development of sulphide structures at the Broken Spur hydrothermal vent site, 29°10'N Mid-Atlantic Ridge, *J. Geol. Soc. London* 155 (1998) 773–785.
- [12] T. Hirata, R.W. Nesbitt, U–Pb isotope geochronology of zircon: evaluation of the laser probe–inductively coupled mass spectrometry technique, *Geochim. Cosmochim. Acta* 59 (1995) 2491–2500.
- [13] R.W. Nesbitt, T. Hirata, I.B. Butler, J.A. Milton, UV laser ablation ICPMS: some applications in the Earth sciences, *Geostand. Newsl.* 20 (1998) 231–243.
- [14] R. Knott, *Hydrothermal Diagenesis*, Unpubl. PhD Thesis, University of Wales, 1995, 299 pp.
- [15] Y. Fouquet, A. Wafik, P. Cambon, C. Mevel, G. Meyer, P.

- Gente, Tectonic setting and mineralogical and geochemical zonation in the Snake Pit sulphide deposit (Mid-Atlantic Ridge at 23°N), *Econ. Geol.* 88 (1993) 2018–2036.
- [16] D. Vaughan, J. Craig, *The Mineral Chemistry of Metal Sulphides*, Cambridge University Press, Cambridge, 1978.
- [17] R.C. Weast (Ed.), *Handbook of Chemistry and Physics*, 53rd ed., The Chemical Rubber Company, Cleveland, OH, 1972, F177–F178.
- [18] D.L. Huston, S.H. Sie, G.F. Suter, D.R. Cooke, R.A. Both, Trace elements in sulphide minerals from eastern Australian volcanic-hosted massive sulphide deposits: part I, Proton microprobe analyses of pyrite, chalcopyrite, and sphalerite, and part II, Selenium levels in pyrite: comparison with $\delta^{34}\text{S}$ values and implications for the source of sulphur in volcanogenic hydrothermal systems, *Econ. Geol.* 90 (1995) 1167–1196.
- [19] A. Wittman, Indium 49-A Crystal Chemistry, in: K.H. Wedepohl (Ed.), *Handbook of Geochemistry*, II/4, Springer, Berlin, 1974, pp. 49-A-1–49-A-8.
- [20] R.A. Mills, J. Thomson, H. Elderfield, R.W. Hinton, E. Hyslop, Uranium enrichment in metalliferous sediments from the Mid-Atlantic Ridge, *Earth Planet. Sci. Lett.* 124 (1994) 35–47.
- [21] J. Thomson, N.C. Higgs, I.W. Croudace, S. Colley, D.J. Hydes, Redox zonation of elements at an oxic/post-oxic boundary in deep-sea sediments, *Geochim. Cosmochim. Acta* 57 (1993) 579–595.
- [22] P. Wersin, M.F. Hochella Jr., P. Perrson, G. Redden, J.O. Leckie, D.W. Harris, Interaction between aqueous uranium (VI) and sulphide minerals: spectroscopic evidence for sorption and reduction, *Geochim. Cosmochim. Acta* 58 (1994) 2829–2844.
- [23] D.C. Harris, L.J. Cabri, R. Nobiling, Silver-bearing chalcopyrite, a principal source of silver in the Izok Lake massive sulphide deposit: confirmation of electron and proton microprobe analyses, *Can. Mineral.* 22 (1984) 493–498.
- [24] R.R. Large, D.L. Huston, P.J. McGoldrick, Gold distribution and genesis in Australian volcanogenic massive sulphide deposits and their significance for gold transport models, *Econ. Geol. Monogr.* 6 (1989) 520–535.
- [25] M.D. Hannington, S.D. Scott, Sulphidation equilibria as guides to gold mineralisation in volcanogenic massive sulphides: evidence from sulphide mineralogy and the composition of sphalerite, *Econ. Geol.* 84 (1989) 1978–1995.
- [26] L.G. Benning, T.M. Seward, Hydrosulphide complexing of Au (I) in hydrothermal solutions from 150–400°C and 500–1500 bar, *Geochim. Cosmochim. Acta* 60 (1996) 1849–1871.
- [27] K.L. Von Damm, Seafloor hydrothermal activity: black smoker chemistry and chimneys, *Annu. Rev. Earth Planet. Sci.* 18 (1990) 173–204.
- [28] R.H. James, H. Elderfield, M.R. Palmer, The chemistry of hydrothermal fluids from the Broken Spur site, 29°N, Mid-Atlantic Ridge, *Geochim. Cosmochim. Acta* 59 (1995) 651–659.
- [29] S. Chenery, J.M. Cook, M. Styles, E.M. Cameron, Determination of the three dimensional distributions of precious metals in sulphide minerals by laser ablation microprobe-inductively coupled plasma–mass spectrometry (LAMP–ICPMS), *Chem. Geol.* 124 (1995) 55–65.